The effects of 180 years of aging on the physical and seismic properties of partially saturated sands

Vanshan Wright[1,2†] and Matthew Hornbach[1]

[1]Southern Methodist University, Roy Huffington Department of Earth Sciences, Dallas, Texas, 75206.

[2]Woods Hole Oceanographic Institution, Department of Geology and Geophysics, Woods Hole, Massachusetts, 02543.

Corresponding author: Vanshan Wright (vwright@whoi.edu)

[†]now at.

Key Points:

- Elastic moduli of recently deposited sands at Port Royal Beach increase with age for at least 180 years
- Time-dependent increases to the elastic moduli of Port Royal sands are not solely explained by mechanical compaction
- Elastic moduli of these sands most likely increase with age due to grain reorganization that leads to higher grain contact friction

Abstract

Constraining how the physical properties and seismic responses of recently deposited sands change with time is important for understanding earthquake site response, subsurface fluid flow, and early stages lithification. Currently, however, there is no detailed (cm-scale) assessment of how sand physical properties and associated seismic velocities evolve over the first two centuries after deposition. Here, we integrate sedimentation rates with seismic velocity and sediment physical properties data to assess how the vadose zone sands at Port Royal Beach, Jamaica, change within 180 years after deposition. We show that compressional and shear wave velocities increase with sediment age, whereas porosity, grain size, sorting, mineralogy, and cementation fraction remain relatively unchanged during the same period. Rock physics models (constrained by the measured physical properties) predict constant seismic velocities at all sites regardless of sediment age, though misfits between modeled and observed velocities increase with sediment age. We explain these misfits by proposing that shallow sands undergo microstructural grain reorganization that leads to a more uniform distribution of grain contact forces with time. Our results imply that beach sands undergo a previously undocumented lithification process that occurs before compaction.

Plain Language Summary

Sands change after being deposited. Their porosity (i.e., volume of pore space) reduces, the average number of grains contacting each other increases, and chemical reactions may cause the grains to adhere more firmly. These changes influence how strong sands are, how resistant they are to being deformed by earthquakes, the ability for fluids flow through sands, and how quickly the transition from sand to solid rock occurs. For many years, scientists believed that

porosity reduction was the dominant non-chemical way sands change and become stronger. Forty years ago, researchers observed something quite enigmatic – the strength of artificial sands increase within minutes after being deposited. This strengthening lasted for three decades and occurred without significant porosity reductions. Until now, it was unclear what controls this process, whether it lasts longer than decades, and whether it occurs in natural beach sands. This paper argues that, within the first 180 years after deposition, natural sands at Port Royal Beach in Jamaica strengthen due to grain rotation, slippage, and rolling that increase contact area and stress between the grains without reducing porosity significantly. The new paradigm developing is that recently deposited shallow sands more significantly change via this grain reorganization process rather than by porosity reduction.

1 Introduction

The physical properties and seismic velocities of shallow sediments vary with depth and time since deposition (Pryor 1973; Atkin & McBride, 1992; Prodger et al., 2016). Variations exist in sediment porosity, density, sphericity, sorting, grain size, rounding, fluid saturation, cement fraction, and seismic velocities (McLean & Kirk, 1969; Pryor 1973; Atkin & McBride, 1992; Gunn et al., 2006; Vousdoukas et al., 2007; Prodger et al., 2016). Variations in sediment properties control subsurface fluid flow and sediment strength and are crucial for understanding slope stability, earthquake-induced liquefaction, seawater intrusion and upwelling, sediment lithification, and the development of oil and gas reservoirs (Morelock 1969; Lundegard 1992; Dugan & Fleming, 2002; Crowe & Mine, 2013).

With increased burial, sediments typically experience effective stress-induced porosity reductions that cause increases in bulk density, the average number of grain-grain contacts per particle (coordination number), elastic moduli, and seismic velocities (Athy, 1930; Murphy, 1982; Grauls & Brévart, 2002; Dutta et al., 2009). This process (mechanical compaction) is well-documented with direct measurements in deep (>100 m) marine sediments (e.g., Athy, 1930; Dutta et al., 2009). However, porosities of well-sorted, medium-grained beach, river, and dune sediments remain constant with depth down to at least 17 m (0.47-0.49 for 174 samples) (Pryor, 1973; Atkins & McBride, 1992). Coordination numbers of these sands slightly increase with depth (from ~1-2 for 50 samples down to 17 m) despite porosities remaining constant (Atkins & McBride, 1992). These observations contradict expectations that porosity reduction is the primary cause of increases in coordination number with depth (Athy, 1930; Murphy, 1982; Revil et al., 2002; Dutta et al., 2009).

Time since deposition influences the physical properties of shallow sediments. Seasonal variations in beach grain size and sorting correlate with changes in sediment source, wind strength, currents, and wave conditions (Prodger et al., 2016). Freshly deposited artificial sands, silt-laden tailing, and sand columns recreated in the lab experience increases to their shear moduli that begin within minutes after deposition, last for days to 1-4 decades, and are not solely attributed to porosity reduction, which is typically less than 3% change in porosity during the same period (Mitchell & Solomayor, 1984; Dumas & Beaton, 1988; Mesri et al., 1990; Troncoso & Graces, 2000). Since the first observation of this processes ~ 40 years ago, studies have hypothesized but have yet to show definitively in the field that time-dependent increases to sediment shear moduli could be the result of increased cementation or grain reorganization that leads to increased friction at grain contacts (Bowman & Soga, 2003; Mitchell, 2008). Presently, it is unclear whether natural clean (< 5 % fines) sands also experience similar age-dependent shear moduli changes, what controls the process, and whether it lasts longer than decades (Mitchell, 2008).

A feasible way to study centennial-scale sediment changes involves making measurements along a coastline-to-inland transect at a prograding beach whose sediment source has not changed for centuries (Figure 1-4). Spatiotemporal sediment changes would be evidenced by statistically significant increases or decreases to seismic velocities and or core-measured properties (porosity, density, grain size, cement fraction, saturation, and mineralogy). It is reasonable to infer that the grain or fluid microstructures are different between study sites if the core-measured physical properties cannot explain changes in seismic velocities. Comparisons between measured and predicted seismic velocities from Hertz-Mindlin's rock physics model (Mindlin, 1949) could provide first-order insights into how changes in the sediments' microstructure influence seismic velocities. This rock physics model approximates sands as randomly organized groups of identical spheres whose grain-contact forces are uniformly distributed and quantifiable using Hertzian-contact mechanics (Mindlin, 1949). Unlike the other six granular media rock physics models where there has been little to no ground-truthing work to understand causes for seismic velocity mispredictions, studies show that mispredictions from Hertz-Mindlin's rock physics models are attributable primarily to nonuniform distributions of contact forces introduced by variations in coordination number, contact geometries, and force chain links in natural sands (Maske et al., 1999; Maske, 2004; Bachrach and Avseth, 2008). By combining Hertz-Mindlin's rock physics model insights into sediment microstructure with coring and seismic velocity data, one achieves a relatively comprehensive way of quantifying spatiotemporal sediment changes.

We perform a cm-scale assessment of how vadose zone sands (upper 2.2 m) at Port Royal Beach, Jamaica, change within 180 years after deposition. This prograding beach is scientifically appropriate for our study because the beach's sediment deposition, erosion, and liquefaction history are well-documented, and there exist legacy maps for constraining sediment age at decadal resolutions (Fuller, 1907; Goreau & Burke, 1966; McDonald et al., 2013). We interpret that its sands experience grain reorganization (i.e., rolling, slipping, and rotation that leads to changes in grain positions and contact geometries) that leads to more uniform distributions of contact forces but no significant changes to porosity. This grain-reorganization process is more dominant than porosity-reducing mechanical compaction at controlling the strength, seismic velocity, and porosity of sands during their first 180 years after deposition.

2 Methods

We use t-tests and Monte-Carlo analyses to identify spatiotemporal changes between sediment age, seismic velocities, and physical properties at four sites (sites1-4) at Port Royal Beach (Figure 1). We constrain sediment ages using legacy maps and topographic surveys. We constrain mineralogy, grain size, sorting, sphericity, roundness, porosity, density, and cement fraction from trench sidewall cores. We measure and model seismic velocities using refraction surveys and Hertz-Mindlin's rock physics model (Mindlin, 1949), respectively.

2.1 Constraining Sediment Age

We constrain sediment age using three-dimensional time contours derived from the beach's paleo shoreline, submarine and subaerial slope surveys, and sea-level curves (Figure 1 and S1). We digitize paleo shorelines from georeferenced maps of Port Royal dated to 1692, 1782, 1785, 1873, 1876, 1887, 1950, 1968, and 1974 using 425-year-old (or older) buildings, roads, and landmarks as control points (e.g., Port Royal Navy Hospital, Fort Charles, St. Peters Anglican Church and High Street). Affine transformations during the georeferencing produce shoreline position uncertainties of 3-13 m. We account for these uncertainties by calculating sediment age for all possible combinations of shoreline positions. Where possible, we also randomly remove 1-2 control points and assess their influences on the shoreline positions. While creating the time contours, we also assume that the submarine and subaerial beach slopes remained constant over the last two centuries because (1) this is what historical elevation and bathymetric maps show, (2) deposition rates were primarily controlled by long-shore drift and easterly winds during this period (Goreau & Burke, 1966; Wright et al., 2019), and (3) Jamaica's local sea level has remained constant for at least 425 years (Digerfeldt & Hendry, 1987). We interpolate between the contours to estimate sediment ages at sites 1-4.

2.2 Sediment Collection and Physical Property Analyses

We dug 1.8-2.2 m deep trenches at sites 1-4 and used aluminum cans (mostly 10 cm high by 6 cm wide) to collect 1-3 sidewall samples from the middle of each sand bed (Figures 2a-2d). We collected a total of 10, 11, 9, and 9 samples from sites 1-4, respectively. After collection, we immediately covered and stored the samples, weighing them within ~1-30 minutes. We dried the samples in an oven for at least 8 hours before re-weighing them to estimate wet and dry weights.

We assessed mineralogical changes using x-ray diffraction (XRD), scanning electron microprobe, optical microscopy, and pictomicrographic analyses. We used the PDF-4+ International Center for Diffraction Data library as a reference for identifying minerals and calculated relative percentages using the reference intensity ratio method (Hillier, 2003). We quality control XRD results by inspecting the unaltered sediments with an optical microscope, pictomicrograph, and a scanning electron microprobe, which help distinguish between detrital calcium carbonate versus cement. We quantified carbonate percentage by measuring sand mass changes after saturating 40-100 g of each sample in 10 percent diluted hydrochloric acid for at least 24 hours.

We estimated grain size and sorting using the Folk and Ward (1957) and a stochastic numerical grain recreation method. First, we used a mechanical shaker and sieving to bin the sediments based on grain size. Approximately 61 % of the samples have bimodal or trimodal grain size distributions, with the remaining 39 % being unimodal. Since the Folk and Ward (1957) method yields erroneous sorting estimates for non-unimodal samples, we also estimated grain size and sorting numerically. We began by approximating the samples as a group of perfect spheres whose total mass equals the weighed mass of the retained sediments in each sieve and whose diameters are within each sieve's range. We performed this analysis 10 000 times, representing the mean grain size as the radius of the mean weighted mass for the entire reconstructed sample and sorting as the weighted standard deviation. The perfect sphere assumption is valid as 30-50 grains from each bed have mean sphericities of 0.7-0.8 on a scale of 0-1, where one refers to a perfect sphere (Figure 3G). Folk and Ward (1957) and our numerical approach produce an average difference in grain size of ~0.2 mm or ~26.2 %. We quantified grain sphericity and roundness using the methods of Zheng & Hyrciw (2015). Sphericity and roundness uncertainties derive from their standard deviations.

We used the samples' mass, volume, and mineralogy to estimate bulk density, porosity, and water saturation. Bulk density is the mass of the wet sand divided by its volume. Porosity is one minus the ratio of samples' bulk and mineral density, and water saturation is the quotient of pore water volume and pore volume. We calculated average mineral densities using the arithmetic mean, assuming that the densities of quartz, albite, and calcite (i.e., the three minerals within the sediments) to be 2.65 g/cm^3, 2.62 g/cm^3, and 2.71 g/cm^3, respectively (Katahara, 1996; Wang et al., 1998; Prasad et al., 2002). The density, porosity, and water saturation uncertainties derive from the variances in mass, volume, and mineralogy.

2.3 Seismic-Refraction Data Collection and Velocity Analysis

We constrained V_p by analyzing the waveforms collected during 24-channel reverse refraction surveys. The geophones have corner frequencies of 4 Hz, the receiver spacing was 0.3 m, and the source offset was 0.3-19 m (incrementing by 3 m). The source was a 16 lb. hammer that strikes an aluminum plate ten times to increase the signal to noise ratio. To create V_p travel-time curves, eight seismologists at Southern Methodist University picked first-arrivals, and the first author picked first-arrivals at 3-5 separate times within three months. We (the authors) estimate V_p (from travel-time curves) using the first-break geometrical method and Wiechert-Herglotz solution for horizontal components of turning wave velocities (Herglotz, 1907;

Wiechert & Geiger, 1901; Batemann, 1910; Wiechert, 1910). We determine velocity uncertainties by randomizing the first-arrival picks used in the travel-time curves.

We estimated V_s using multichannel analyses of the surface waves collected during 24-channel refraction surveys with receiver spacings and shot offsets of 1.5 m and 7 m, respectively. We calculated dispersion curves using the phase shift method (Park et al., 1999) and inverted for V_s structure using Geopsy's (www.geopsy.org) neighborhood algorithm (Wathelet et al., 2004). We perform three sets of inversion per dispersion curve – these inversions run for 25000, 35000, or 50000 times. Each new inversion begins with 5000 randomly generated models that are constrained by the dispersion curve and empirical relationships between V_s and surface wave dispersion. Specifically, we set V_s to respectively 1 and 1.16 times the minimum and maximum phase velocity of the surface waves (consistent with Richart et al., 1970), V_p to 150-2500 m/s, Poisson's ratio to 0.2-0.5, and density to 1500 g/cm^3. We use Cox and Teague (2016)'s layer ratio method to create five separate layer thickness input models. We set the depth of the shallowest and deepest layer to 0.2-0.3 times the minimum and maximum wavelength of the surface waves, respectively. The thickness of the layers beneath the shallowest one consistently increases by a ratio of either 1.2, 1.4, 1.6, 1.8, or 2.0 times the thickness of the shallowest layer. We did not use measured bed thickness to constrain the solutions because doing so would overparameterize an already non-unique and ill-posed inversion problem; beds are not resolvable with the seismic data because the beds are smaller than 0.2 times the minimum wavelength of the surface waves. After using the Haskell-Thomson method (Thomson, 1950; Haskell, 1951) to calculate dispersion curves for the proposed model solutions, we calculate the misfits between modeled and observed dispersion curve using the root mean squared error before performing 5000 random walks, which functions to avoid local minima when a new set of 5000 models are generated. Our solutions are the 1000 best-fit models taken from the layer thickness model with the lowest corrected Akaike information criteria score.

2.4 Seismic Velocity Predictions from Rock Physics Modeling

We calculate compressional and shear wave velocities using equations 1-2, where ρ_b, K_{eff} and μ_{eff} represent bulk density, effective bulk modulus, and effective shear modulus, respectively. We estimate K_{eff} and μ_{eff} from Hertz-Mindlin's rock physics model (Mindlin, 1949; equations 3-9) and Biot-Gassmann theory (Gassmann 1951; Biot, 1956; equation 10). ρ_b is from the sediment core analyses.

$$Vp = \sqrt{\frac{\frac{4}{3}\ K_{eff} +\ \mu_{eff}}{\rho_b}} \tag{1}$$

$$Vs = \sqrt{\frac{\mu_{eff}}{\rho_b}} \tag{2}$$

Hertz-Mindlin provides estimates on dry-frame bulk and shear moduli. The model requires (1) porosity $\emptyset_z$, (2) effective pressure P_{eff} estimated from equation 5 where g, ρ_b, z, W_d, Y_w and S_w respectively refer to acceleration due to gravity, bulk density, sample depth, water depth, unit weight of water, and fluid saturation percentage, (3) mineral bulk k_m and shear μ_m derived from Voigt M_v and Reuss M_R bounds (i.e., equations 6-7 where f_i and m_i respectively refer to fractional proportion and elastic moduli of the i^{th} mineral) (Hill, 1952), (4) mineral poisons ratio η_m derived from equation 8, (5) average coordinate numbers c derived from equation 9 (Murphy, 1982), and the volume fraction of rough to smooth grain contacts ft, where rough (smooth) grain contacts are ones that resist entirely (allows) tangential slip during seismic wave propagation.

$$K_{HM} = \left[\frac{c^2(1-\emptyset_z)^2 {k_m}^2}{18\pi^2(1-\eta_m)^2} P_{eff}\right]^{\frac{1}{3}} \tag{3}$$

$$\mu_{HM} = \frac{2+3ft-\eta_m(1+3ft)}{5(2-\eta_m)}\left[\frac{3c^2(1-\emptyset_z)^2(4){\mu_m}^2}{2\pi^2(1-\eta_m)^2} P_{eff}\right]^{\frac{1}{3}} \tag{4}$$

$$P_{eff} = g\int_0^z \rho_b(z)\,dz - [z-W_d]S_w Y_w \tag{5}$$

$$M_v = \sum_{i=1}^{N} f_i m_i \tag{6}$$

$$\frac{1}{M_R} = \sum_{i=1}^{N} \frac{f_i}{m_i} \tag{7}$$

$$\eta_m = \frac{3k_m - 2\mu_m}{6k_m + 2\mu_m} \tag{8}$$

$$c = 20 - 34\emptyset_z + 14{\emptyset_z}^2 \tag{9}$$

We used the Gassmann-Biot theory (Gassmann, 1951; Biot, 1956; equation 10) to calculate the effects of fluid saturation on dry-frame bulk moduli. This method assumes that sediments are heterogeneous and fluids are not flowing (Biot, 1956; Gassmann, 1951). In the equation, K_{air} represents the bulk filled sediments (0 kPa) and K_{f2} represents the bulk modulus of the mix of seawater (2.3 GPa) and air. We determine bulk moduli using equation 6-7.

$$\frac{K_{eff}}{K_m - K_{eff}} - \frac{K_{f2}}{\emptyset_z(K_m - K_{f2})} = \frac{K_{HM,W}}{K_m - K_{HM,W}} + \frac{K_{air}}{\emptyset_z(K_m - K_{air})} \tag{10}$$

From equations 1-10, we calculated seismic velocities 10 000 times using parameters and assumptions that minimize uncertainties that arise from using core-point measurements to predict bulk-averaged measured seismic velocities within each trench. For each calculation, we randomly select new parameter values that are between the maximum and minimum estimates of all point measurements of the input parameter per bed (e.g., $\emptyset_z$ and ρ_b). We assume that the point measurements could have been taken at any depth within each bed and assign one velocity per bed per iteration. We assume that grains could be organized anywhere between their strongest and weakest configurations. Finally, we infer changes to the sediment microstructure by comparing measured versus predicted seismic velocities (Bachrach & Avseth, 2008).

3 Results

3.1 Sediment Age and Deposition Rate

All analyzed Port Royal Beach sediments were deposited between 1692-2017. During this time, the shoreline prograding at an average rate of 0.3-0.48 m/year except between the years 1782-1786, 1873-1888, and 1968-1975 which experienced shoreline erosion (Figure S2). The highest and lowest progradation rates occurred between 1951-1968 (4.6±0.24 m/year) and 1692-1782 (0.3±0.06 m/year), respectively. Progradation rates during the deposition of the sediments at sites 1-4 were 1.05±0.1, 4.6±0.24, 2.3±0.11, and 1.18±0.0 m/year, respectively (Figure S2).

Analysis of the time contours created by shoreline position and slopes reveals (Figures 1 and S1) that sites 1-4's sediments were deposited within the last ~180 years. Site 1-4's sediments were deposited between 1988-2016, 1956-1974, 1909-1923, and 1837-1862 respectively. During these periods, average sedimentation rates within the upper 2 m of the subsurface ranged from 5-25 cm/year. The average calculated sedimentation at site 1-4 was 6-7 cm/year, 9-11 cm/yr, 14-25 cm/year, and 5-11 cm/year, indicating that sedimentation rates were fastest during the deposition of lines 2 and 3.

3.2 Sediments Physical Properties

The sediment type, subsurface stratigraphy, ground surface condition, and water table depth are similar between study sites. Specifically, sites 1-4 are mostly made up of olive, white, yellow, and tan colored siliciclastic sands stratified into individual beds based on grain sizes, mineralogy, porosities, and densities (Figure 2). There are 9, 8, 7, and 7 individual beds at sites 1-4, respectively. Grass has grown atop sites 3-4, but its roots are not anchored more than 5 cm beneath the subsurface (Figures 1 and 2). The water table was between 1.9-2.2 m at all sites during trenching.

The composition (mineralogy, cement fraction, grain size, and grain shape) of the sediments at sites 1-4 are similar. The minerals are predominantly albite, quartz, and calcite; grains are rounded to well-rounded, mostly spherical and, their sizes ranged from coarse to very coarse sands (Figure 3). When uncertainties are considered, statistical analyses reveal that it is more probable that the average values of these physical properties are indistinguishable (within a 50-50 probability) from each other than that they change between sites. The lone exception is a 0.82 probability that site 1's bulk modulus is larger than sites 2-3's. The higher bulk modulus at line 1 reflects a relatively larger percentage of albite at site 1, which is 77.2 % compared to sites 2-4 average albite percentages of 45.9 %, 45.7 %, and 63.4 %, respectively.

Average porosities and densities are constant within the average ~5% uncertainty, with sites 2-4 porosities and densities being respectively within 0.01 and 0.04-0.14 g/cm^3 of site 1's. Though differences exist at the individual depth, statistical analyses also show no detectable increasing trends with time across all four sites either as a function of depth or as a function of the averages at each site. Instead, the analyses show that it is more probable that these physical properties are also indistinguishable between sites as the probabilities that these physical properties increase or decrease with age are within 0.1-0.17 of 0.5 probabilities (i.e., a 50:50 chance). The pores are filled with relatively small water quantities (0-0.6% with a mean of 0.1%). The saturation percentage between sites 1-3 is statistically indistinguishable as a function of depth (Figure 3J), whereas there is a 0.35 probability that site 1-3's water saturation is higher than site 4's (Table 1).

3.3 Sediments' Observed and Predicted Seismic Velocities

All measured seismic velocities (i.e., phase velocities of the surface waves, Vp, and Vs) increase between sites 1-2 and 3-4 (Figure 2e-2g). Seismic velocities are indistinguishable between sites 1 and 2 and between sites 3 and 4. Changes to Vp show the most complexity in space and time (Figures 2f and 2g). Within the upper 1m, turning wave velocity inversion reveals that Vp increases from sites 1-3 (Figure 2g). At the surface, Vp for site 4 is lower than at sites 1-3 but becomes faster than sites 1-2 with depth (starting at 1 m). Turning wave velocity results also show that Vp increases with time between 1-2 m. In contrast, the first-break geometric method shows that Vp in the upper 0.3 m does not increase with time (Figure 2f) and that Vp within the upper 0.3-1 m is roughly the same but increases with time between sites 1-2 and 3-4 at depths between 1-2 m. Overall, the Vp reveal a clear increasing Vp trend between sites 1-2 and 3-4 can only be resolved at depths of 1-2 m. Vs increases faster than Vp.

Rock physics models predict that seismic velocities are statistically indistinguishable at all sites (Figure 4I-J). Misfits between modeled and observed seismic velocities decrease with age, and models assuming infinite slip at all grain contacts (i.e., 100 % smooth-grained models) generally perform better than those assuming no slip at grain contacts (i.e., 100 % rough-grained models) (Figure 4). The 100% rough-grained models overpredict velocities except for V_p at site 3 and below 1.2 m at site 4 (Figure 4).

4 Discussion

The relationships between measured and modeled velocities at Port Royal Beach sometimes conflict. Below, we demonstrate that changes to the measured physical properties do not explain the discrepancies in measured and modeled velocities. Instead, we propose that seismic velocities increase with age due to grain reorganization, which increases the sands' elastic moduli.

Spatiotemporal increases to seismic velocities at Port Royal Beach (Figure 2) provide evidence that at least one physical property at Port Royal Beach changes with age. Variation and uncertainty in the average mineral moduli, porosity, density, fluid saturation, and cement fraction alone cannot explain increases to seismic velocities as (1) there are no sustained and statistically significant changes in the site-wide averages of these properties and (2) rock physics model-predicted velocities are statistically indistinguishable when the combined effects of all variations (average or at individual depth levels) in these properties are considered (Figure 4I-4J). We discard patchy fluid saturation because it does not explain the increases to V_s (Gassman, 1951). We also discard porosity reduction and pore space cement because the rock physics models estimate that, when all else equal, at least a 20-30 % decrease in porosity at sites 3-4 is needed to account for seismic velocity increases. It is unlikely that all cements are at grain contacts and or surround the grains because this would lead to seismic velocities that are larger (by ~500-1000 m/s) than what we measure (Avseth et al., 2009). We are skeptical that a mixed distribution of cements (some within pore spaces and some at contacts) is responsible for increasing velocities because there are no statistically significant changes to cement percentage with time, the depositional condition at the sites has remained relatively constant with time (Goreau and Burke, 1966), and assuming that cements are within the pore space better predict seismic velocities at all sites.

Instead of changes to porosity and or cement fraction, an alternative hypothesis is that grain contact force distribution becomes more uniform with time and is responsible for increasing seismic velocities at Port Royal Beach. Support for this hypothesis comes from the observations that the models' misfits decrease with age, a finding which implies that the primary model assumptions (i.e., grains are identical and forces are equally distributed between grains) are more appropriate in the older sands. Observations that the 100 % smooth grain models predict V_p and V_s more accurately than the rough-grained models at sites 1-2 but begins to underpredict V_p beneath 1.2 m at sites 4 are also instructive. These results indicate that increases in grain-contact friction are unlikely to be the primary or only cause of the observed time-dependent increases to seismic velocities at Port Royal Beach (Figure 4; Walton, 1987). Seismic velocity increases could, therefore, be caused by a combination of increases in the uniformity of distributed grain-contact forces and relatively smaller changes to friction at grain contacts (Figure 4).

Changes to grain contact forces can only occur if grains undergo microstructural readjustments (e.g., grain rolling, sliding, and rotating) with time. Grain readjustments may be induced by several processes, including but not limited to natural and anthropogenically introduced stresses such as earthquakes, sub-surface fluid flow during intense rainfall, nearshore seawater waters, and human activities that vibrate sands. Grain readjustments can also occur via contact creep, which is defined as microstructural grain readjustments that occur (without significant external forcing) along naturally existing grain asperities or localized instabilities (Figure 4L-M) as a means of reducing potential energy within granular systems. The former groups of readjustment processes (e.g., vibration loading processes such as earthquakes or waves hitting the coasts) are often accompanied by porosity reduction. In contrast, discrete element models and lab-tests show that, in the absence of external forcing, contact creep alone can lead to increases in sediment elastic moduli that cannot be solely attributed to porosity reduction, which is typically less than 1.7 % when modeled (Bowman & Soga, 2003; Wang et al., 2008). As these numerical models and lab tests were done at confining pressures of 400-500 kPa, it is unclear whether this represents a one-to-one relationship with the vadose zone sediments at Port Royal Beach (Bowman & Soga, 2003; Wang et al., 2008). Noteworthy, however, is that the high porosities, moderate sorting, and high sphericity at Port Royal Beach would form a relatively good environment where grains can more freely rotate, roll, and slip along naturally existing surface asperities or at nonuniform grain contacts, thus creating more stable grain contacts between the same or previously non-contacting grains (see Figure 4L-M; Wang et al., 2014). Also noteworthy is that when sands are unloaded from 500 kPa to 50 kPa, grain rotations continue to occur (Bowman & Soga, 2003), suggesting that grain readjustment occurs in relatively lower effective stress environments. Our preferred interpretation is, therefore, that contact creep-induced grain reorganization is likely leading to increases to the grain contact area and homogenization of grain contact force chains, which is the primary cause for increases to seismic velocity with time without significantly reducing porosities.

The primary finding of this work (i.e., sands experience time-dependent increases to their elastic moduli that cannot be solely explained by porosity reduction) is consistent with prior studies of spatiotemporal changes to natural and artificial sands. To our knowledge, this work represents the first natural evidence suggesting that, for at least 180 years, the shear strength, elastic moduli, and microstructure of recently deposited sands may be controlled by contact creep-induced grain reorganization that does not significantly reduce porosity. These findings imply that there is likely an intermediary process between deposition and mechanical compaction at Port Royal Beach. Here, we propose that contact creep-induced grain reorganization is also a plausible explanation for why the beach, river, and dune sands examined by Atkins & McBride (1992) experience increases in their coordination numbers with depth without significant porosity reduction. As suspected by previous studies, contact creep-induced grain reorganization is also likely responsible for why artificial sands and silt-laden dams experience increases to their elastic moduli with time without significant porosity reduction (Mitchell & Solomayor, 1984; Dumas & Beaton, 1988; Mesri et al., 1990; Troncoso & Graces, 2000). Instead of solely causing increases to grain contact friction, we propose that changes to grain contact area may also increase the elastic moduli of sands. Since the microstructure of shallow sands control subsurface fluid flow and resistance to earthquake-triggered slope instability, an implication of our study is that contact-creep is more dominant than porosity-reducing mechanical compaction at controlling slope stability. Lastly, we predict that our main findings are likely replicable at other Holocene beaches because Port Royal Beach's porosities, densities, grain sizes, and coastline progradation rates (Figure S1) are similar to other Holocene beaches across the world (McLean & Kirk, 1969; Pryor 1973; Atkin & McBride, 1992; Gunn et al., 2006; Prodger et al., 2016; McDonald, 2013).

5 Conclusions

Port Royal Beach, Jamaica, is composed of highly porous albite and quartz-rich sands with less than 3% carbonate cementation. The sands were deposited between 1692 to the present. The compressional and shear wave velocities at the beach increase with sediment age and are unaccompanied by any sustained and statistically significant or detectable increases or decreases to porosity, density, grain size, sorting, and cement fraction with time. Rock physics models more accurately predict seismic velocities for older and deeper buried sands, a discrepancy that cannot be explained when the most liberal uncertainties are employed at each site. Together with the sediment property and seismic velocity analyses, the rock physics model results imply that increasing velocities are better explained by grain reorganization (e.g., rotation and slippage), leading to an increase in the elastic moduli of the sediment matrix with time since deposition.

Our observations are consistent with recent (within the last 40 years) findings by geotechnical engineers, who recognized that artificial sands experience a temporal (within minutes and last for decades) increase in the shear moduli that is accompanied by a relatively small (> 3 %) decrease in porosity. Here, we provide the evidence that this process may also include changes to bulk moduli, occurs within naturally occurring siliciclastic sands, and occurs on not just decadal but on centennial time scales as well. We propose that this process occurs via contact creep primarily, leads to an increase in the magnitude and uniformity of distributed grain contact forces, and represents an intermediary process between sediment deposition and mechanical compaction.

Acknowledgments

We thank Lyndon Brown, Jovan Burton, Shane Cuff, Warren Harding, Sheldon Hoppins, Devere Kennedy, Rajay Mitchell, Paul Parchment, and Damion Phillpotts for helping during field surveys. We collected seismic refraction data using Pascal Instrument Center's equipment. The Society of Exploration Geophysicist Geoscientists Without Borders grant and the Institute for Earth, Science, and Man at SMU partially supported this work.

References

Atkins, J. E., & McBride, E. F. (1992). Porosity and Packing of Holocene River, Dune, and Beach Sands (1). *AAPG Bulletin*, 76, doi: 10.1306/bdff87f4-1718-11d7-8645000102c1865d

Avseth, P., Jørstad, A., Wijngaarden, A., & Mavko, G. (2009). Rock Physics Estimation of Cement Volume, Sorting, and Net-to-Gross in North Sea Sandstones. *The Leading Edge*, 28, 98–108, doi:10.1190/1.3064154

Bachrach, R., & Avseth, P. (2008). Rock physics modeling of unconsolidated sands: Accounting for nonuniform contacts and heterogeneous stress fields in the effective media approximation with applications to hydrocarbon exploration. *Geophysics*, 73, doi: 10.1190/1.2985821

Beard, D.C., & Weyl, P.K. (1973). Influence of texture on porosity and permeability of unconsolidated sand. *AAPG Bulletin*, 57(2), 349–369, https://doi.org/10.1306/819A4272-16C5-11D7-8645000102C1865D

Bowman, E.T., & Soga, K. (2003). Creep, Ageing and Microstructural Change in Dense Granular Materials. *Soils and Foundations*, v. 43,107–117, doi: 10.3208/sandf.43.4_107

Crowe, A., & Milne, J. (2013). Relationship between dry and wet beach ecosystems and E. coli levels in groundwater below beaches of the Great Lakes, Canada. *IAH - Selected Papers on Hydrogeology Groundwater and Ecosystems*, 237–251, doi: 10.1201/b15003-20

Digerfeldt, G., & Hendry, M. D. (1987). An 8000 year Holocene sea-level record from Jamaica: Implications for interpretation of Caribbean reef and coastal history. *Coral Reefs*, 5(4), 165–169, https://doi.org/10.1007/bf00300959

Dugan, B., & Flemings, P.B. (2002). Fluid flow and stability of the US continental slope offshore New Jersey from the Pleistocene to the present. *Geofluids*, 2, 137–146, doi: 10.1046/j.1468-8123.2002.00032.x

Dumas, J.C., & Beaton, N.F. (1988). Discussion of "Practical Problems from Surprising Soil Behavior" by James K. Mitchell (March, 1986, Vol. 112, No. 3). *Journal of Geotechnical Engineering*, 114, 367–368, doi: 10.1061/(asce)0733-9410(1988)114:3(367).

Dutta, T., Mavko, G., Mukerji, T., & Lane, T. (2009). Compaction trends for shale and clean sandstone in shallow sediments, Gulf of Mexico. *The Leading Edge*, 28, 590–596, doi: 10.1190/1.3124935

Fuller, M.L. (1907). Notes on the Jamaica Earthquake. *The Journal of Geology*, 15, 696–721, doi: 10.1086/621461

Goreau, T., & Burke, K. (1966). Pleistocene and Holocene geology of the island shelf near Kingston, Jamaica. *Marine Geology*, 4, 207–224, doi: 10.1016/0025-3227(66)90021-1

Gunn, D., Pearson, S., Chambers, J., Nelder, L., Lee, J., Beamish, D., Busby, J., Tinsley, R., & Tinsley, W. (2006). An evaluation of combined geophysical and geotechnical methods to characterize beach thickness. *Quarterly Journal of Engineering Geology and Hydrogeology*, 39, 339–355, doi: 10.1144/1470-9236/05-038

Haskell, N. A. (1951). The dispersion of surface waves on multilayered media. *Bulletin of the Seismological Society of America*, 43(1), 1–18.

Lundegard, P. D. (1992). Sandstone porosity loss; a" big picture" view of the importance of compaction. *Journal of Sedimentary Research*, 62, 250-260, doi:10.1306/D42678D4-2B26-11D7-8648000102C1865D

Makse, H.A., Gland, N., Johnson, D.L., & Schwartz, L. (2004). Granular packings: Nonlinear elasticity, sound propagation, and collective relaxation dynamics. *Physical Review E*, 70, doi: 10.1103/physreve.70.061302

Makse, H.A., Gland, N., Johnson, D.L., & Schwartz, L.M. (1999). Why Effective Medium Theory Fails in Granular Materials. *Physical Review Letters*, 83, 5070–5073, doi: 10.1103/physrevlett.83.5070

McDonald, R., Wright, V., Hornbach, M.J., Carris, G., Flynn, C., Frone, Z., Fontana, J., Giddens, E., Klausen, A., Mattingly, B., Mauroner, C., Phrampus, B., Brown, L., Mann, P., et al. (2013). *New insights into geohazard risks in Jamaica, Haiti, and the Dominican Republic: A compendium of recent Geoscientists without Borders results*. Paper presented at the SEG Technical Program Expanded Abstracts 2013, Houston, TX, doi: 10.1190/segam2013-1293.1

Mclean, R.F., & Kirk, R.M. (1969). Relationships between grain size, size-sorting, and foreshore slope on mixed sand - shingle beaches. *New Zealand Journal of Geology and Geophysics*, 12, 138–155, doi: 10.1080/00288306.1969.10420231

Mesri, G., Feng, T.W., & Benak, J.M. (1990). Postdensification Penetration Resistance of Clean Sands. *Journal of Geotechnical Engineering*, 116, 1095–1115, doi: 10.1061/(asce)0733-9410(1990)116:7(1095)

Mindlin, R. D. (1949). Compliance of elastic bodies in contact. *Journal of Applied Mechanics*, 16, 259–268, doi: 10.1007/978-1-4613-8865-4_24

Mitchell, J. K. (2008). *Aging of sand–a continuing enigma?* Paper presented at the 6th International Conference on Case Histories in Geotechnical Engineering, Arlington, VA.

Mitchell, J.K. & Solymar, Z.V. (1984). Time-dependent strength gain in freshly deposited or densified sand. *Journal of Geotechnical Engineering*, 110, 1559-1576, doi: 10.1061/(ASCE)0733-9410(1984)110:11(1559)

Morelock, J. (1969). Shear strength and stability of continental slope deposits, western Gulf of Mexico. *Journal of Geophysical Research*, 74, 465–482, doi: 10.1029/jb074i002p00465

Murphy, W.F. (1982). Effects of microstructure and pore fluids on the acoustic properties of granular sedimentary materials, (Doctoral dissertation). Stanford, CA: Stanford University.

Prodger, S., Russell, P., Davidson, M., Miles, J., & Scott, T. (2016). Understanding and predicting the temporal variability of sediment grain size characteristics on high-energy beaches. *Marine Geology*, 376, 109–117, doi: 10.1016/j.margeo.2016.04.003

Pryor, W. A. (1973). Permeability-Porosity Patterns and Variations in Some Holocene Sand Bodies. *AAPG Bulletin*, 57, doi: 10.1306/819a4252-16c5-11d7-8645000102c1865d

Revil, A., Grauls, D., & Brévart, O. (2002). Mechanical compaction of sand/clay mixtures. *Journal of Geophysical Research: Solid Earth*, 107, doi: 10.1029/2001jb000318

Schmertmann, J.H. (1991). The Mechanical Aging of Soils. *Journal of Geotechnical Engineering*, 117, 1288–1330, doi: 10.1061/(asce)0733-9410(1991)117:9(1288)

Thomson, W. T. (1950). Transmission of Elastic Waves through a Stratified Solid Medium. *Journal of Applied Physics*, 21(2), 89–93.

Troncoso, J., & Garcés, E. (2000). Ageing effects in the shear modulus of soils. *Soil Dynamics and Earthquake Engineering*, 19, 595–601, doi: 10.1016/s0267-7261(00)00066-x

Vousdoukas, M., Velegrakis, A., & Plomaritis, T. (2007). Beachrock occurrence, characteristics, formation mechanisms and impacts. *Earth-Science Reviews*, 85, 23–46, doi: 10.1016/j.earscirev.2007.07.002

Walton, K. (1987). The effective elastic moduli of a random packing of spheres. *Journal of the Mechanics and Physics of Solids*, 35, 213–226, doi: 10.1016/0022-5096(87)90036-6

Wang, Y.-H., Lau, Y.M., & Gao, Y. (2014). Examining the mechanisms of sand creep using DEM simulations. *Granular Matter*, 16, 733–750, doi: 10.1007/s10035-014-0514-4

Wang, Y.-H., Xu, D., & Tsui, K.Y. (2008). Discrete Element Modeling of Contact Creep and Aging in Sand. *Journal of Geotechnical and Geoenvironmental Engineering*, 134, 1407–1411, doi: 10.1061/(asce)1090-0241(2008)134:9(1407)

Wang, Z. (2017). Contact maturing and aging of silica sand, (Doctoral dissertation). Retrieved from Deep Blue. (http://hdl.handle.net/2027.42/136992). Ann Arbor, MI: University of Michigan.

Wright, V., Hornbach, M., Brown, L., McHugh, C., & Mitchell, S. (2019). Neotectonics of Southeast Jamaica Derived from Marine Seismic Surveys and Gravity Cores. *Tectonics*, 38, 4010–4026, doi: 10.1029/2019tc005806

FIGURE CAPTIONS

Figure 1. (A) Map of Port Royal Beach. (B) Map showing shoreline positions and transects where we estimate progradation rates (Figure S1).

Figure 2. (A-D) Photos show trench sites 1-4. (E). Surface wave tomography-based (Figure S2) V_s. (F) V_p estimated with Wiechert-Herglotz solution (Tau-p). (G). V_p based on the first-break geometric method.

Figure 3. (A-I) Core physical properties results with 1-sigma uncertainties -- also see Figure S3 and Table S1.

Figure 4. (A-H) Measured versus modeled velocities. (I-J) Comparisons between all modeled velocities. (K) Grain contact scenarios and their effects on model predictions (Bachrach and Avseth, 2008). Dotted lines define circles associated with the grains' radii of curvatures. (L-M) Contact creep illustrations with two possible resulting contact scenarios (Wang, 2017).

Figure 1.

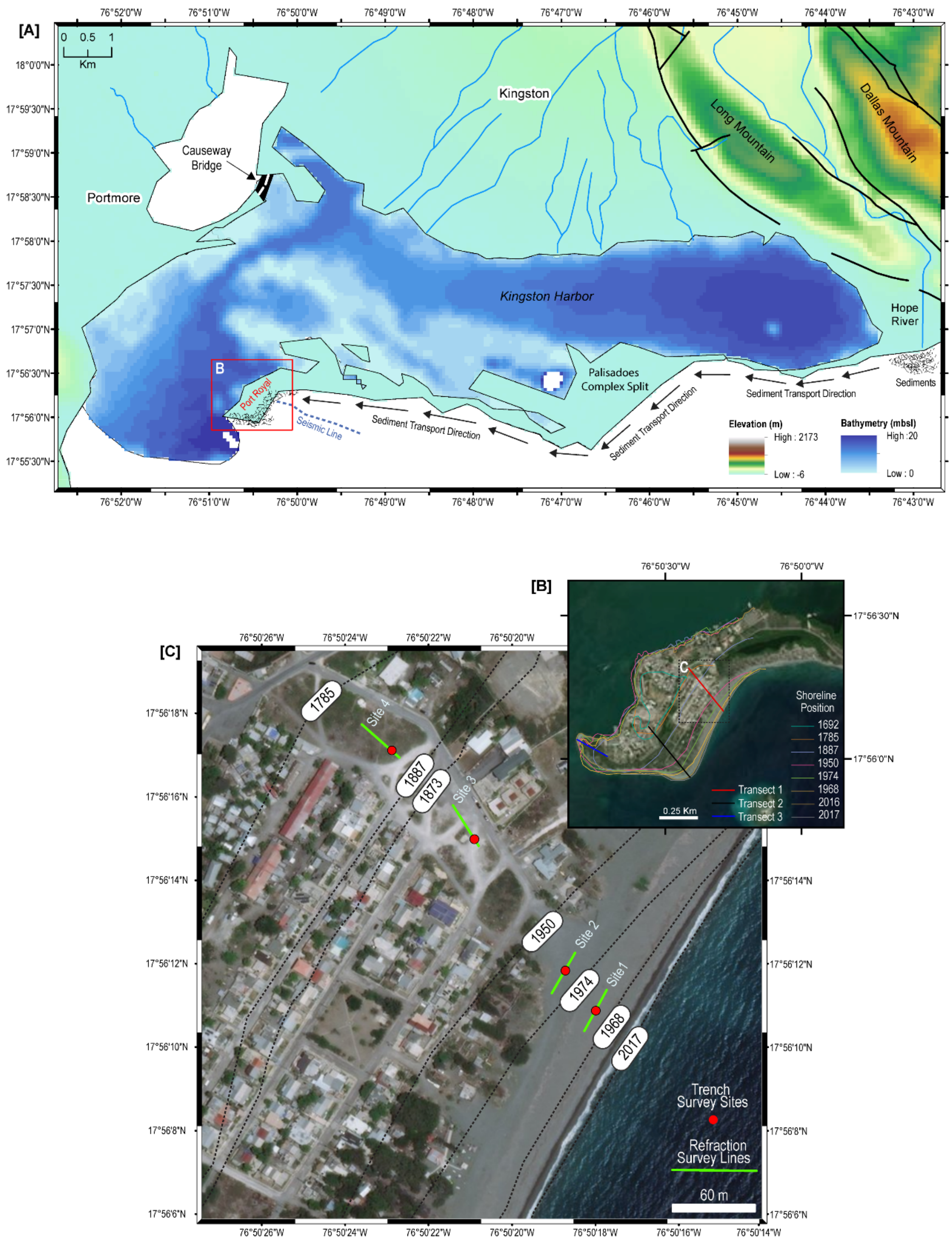
[A]
Km
Kingston
Long Mountain
Dallas Mountain
Causeway Bridge
Portmore
Kingston Harbor
Hope River
Palisadoes Complex Split
Port Royal
Seismic Line
Sediment Transport Direction
Sediments
Elevation (m)
High : 2173
Low : -6
Bathymetry (mbsl)
High :20
Low : 0
[B]
Shoreline Position
1692
1785
1887
1950
1974
1968
2016
2017
Transect 1
Transect 2
Transect 3
0.25 Km
[C]
1785
1887
1873
1950
1974
1968
2017
Site 1
Site 2
Site 3
Site 4
Trench Survey Sites
Refraction Survey Lines
60 m

Figure 2.

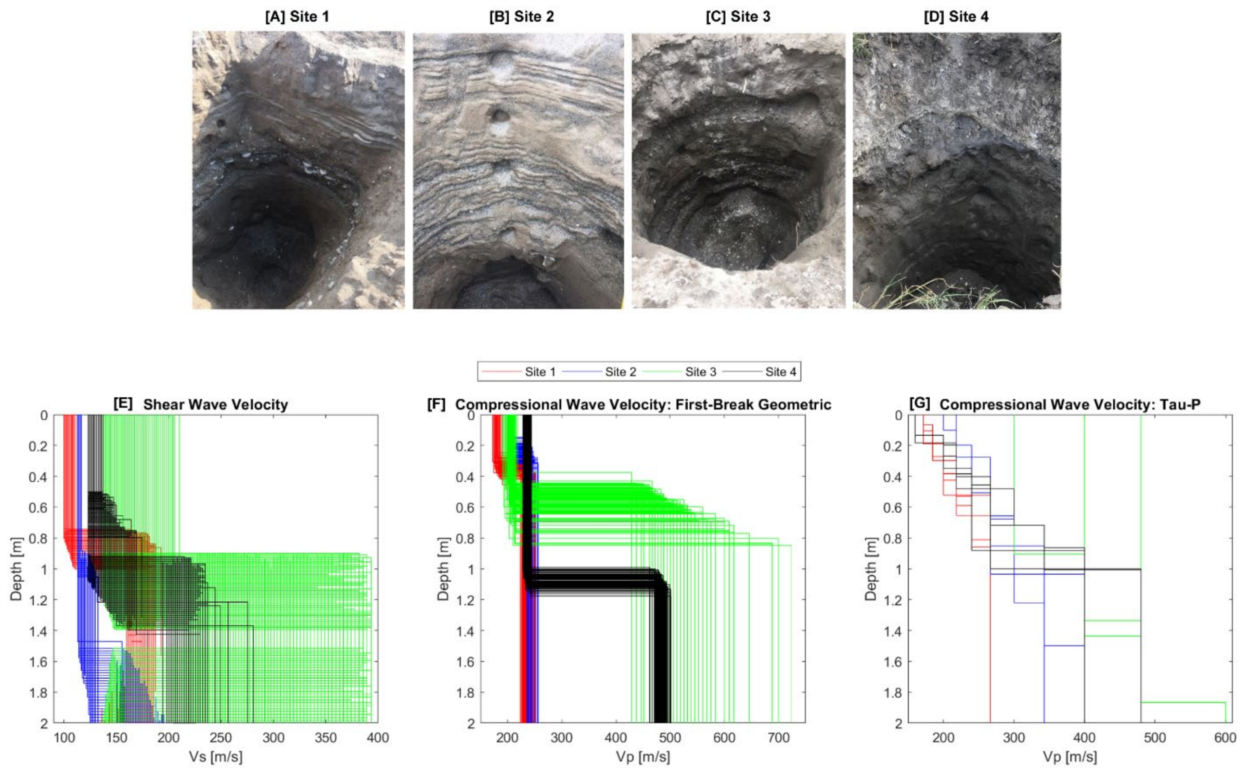

[A] Site 1
[B] Site 2
[C] Site 3
[D] Site 4
Site 1
Site 2
Site 3
Site 4
[E] Shear Wave Velocity
Depth [m]
Vs [m/s]
[F] Compressional Wave Velocity: First-Break Geometric
Depth [m]
Vp [m/s]
[G] Compressional Wave Velocity: Tau-P
Depth [m]
Vp [m/s]

Figure 3.

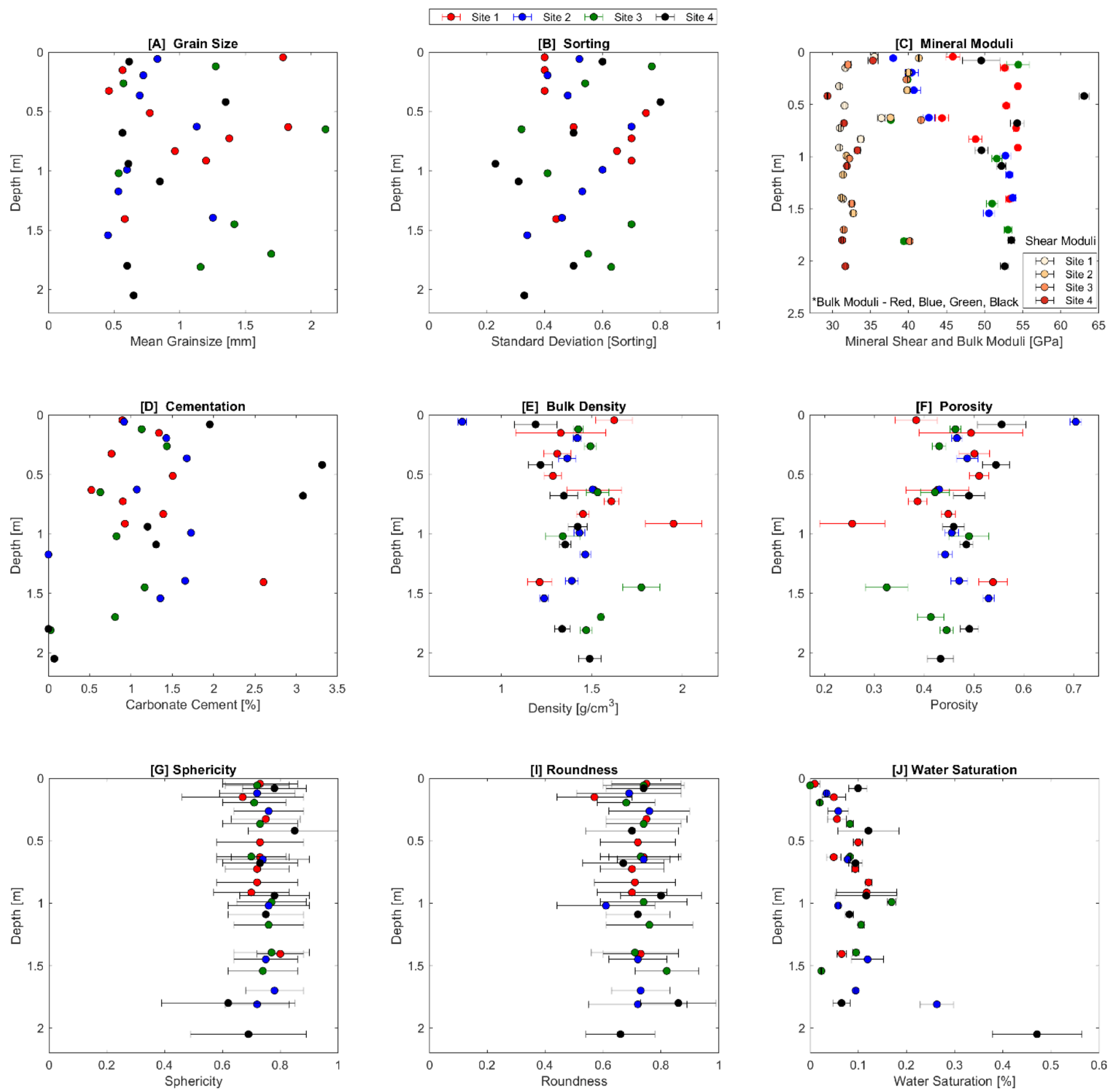

Site 1
Site 2
Site 3
Site 4
[A] Grain Size
Mean Grainsize [mm]
Depth [m]
[B] Sorting
Standard Deviation [Sorting]
[C] Mineral Moduli
Mineral Shear and Bulk Moduli [GPa]
Shear Moduli
*Bulk Moduli - Red, Blue, Green, Black
[D] Cementation
Carbonate Cement [%]
[E] Bulk Density
Density [g/cm3]
[F] Porosity
Porosity
[G] Sphericity
Sphericity
[I] Roundness
Roundness
[J] Water Saturation
Water Saturation [%]

Figure 4.

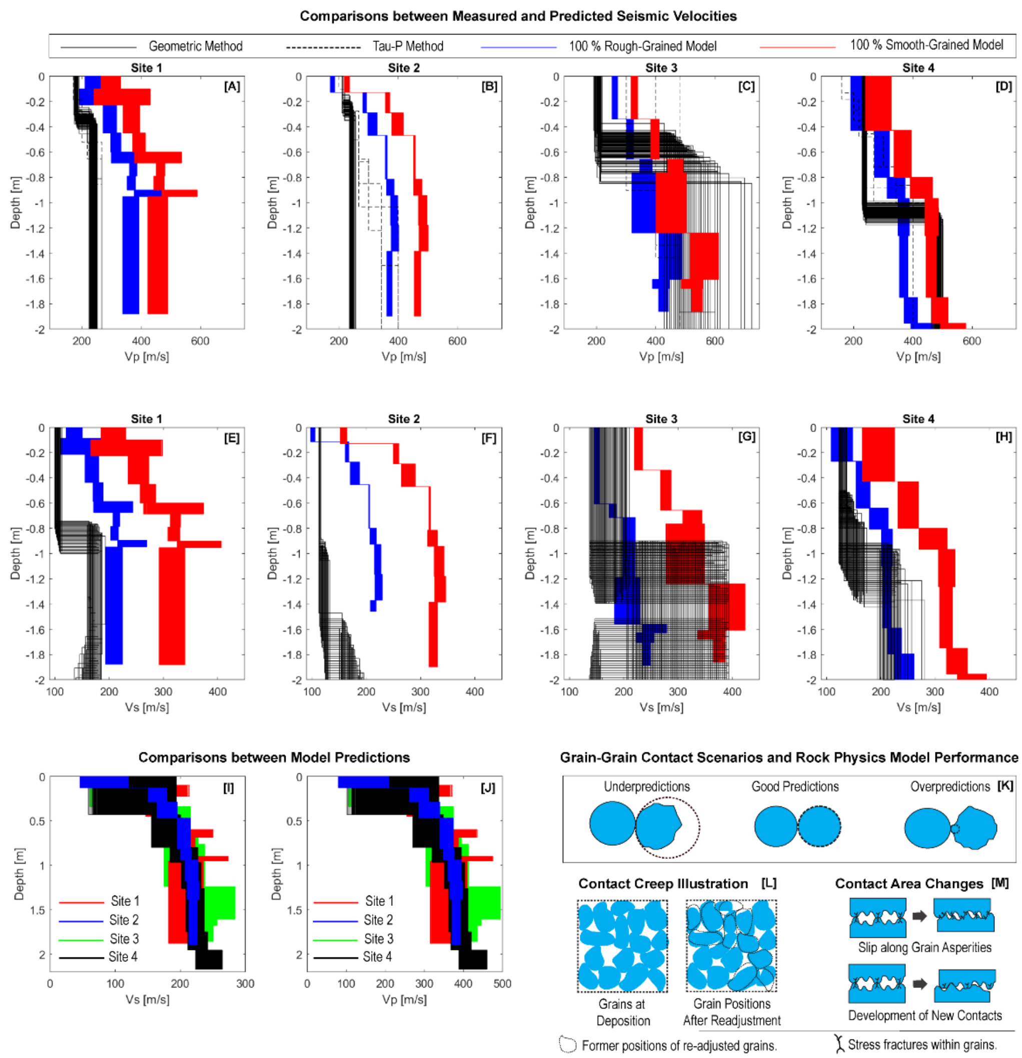

Comparisons between Measured and Predicted Seismic Velocities
Geometric Method
Tau-P Method
100 % Rough-Grained Model
100 % Smooth-Grained Model
Site 1
Site 2
Site 3
Site 4
[A]
[B]
[C]
[D]
[E]
[F]
[G]
[H]
Depth [m]
Vp [m/s]
Vs [m/s]
Comparisons between Model Predictions
[I]
[J]
Grain-Grain Contact Scenarios and Rock Physics Model Performance
Underpredictions
Good Predictions
Overpredictions
[K]
Contact Creep Illustration
[L]
Grains at Deposition
Grain Positions After Readjustment
Contact Area Changes
[M]
Slip along Grain Asperities
Development of New Contacts
Former positions of re-adjusted grains.
Stress fractures within grains.

Journal of Geophysical Research: Solid Earth

Supporting Information for

The effects of 180 years of aging on the physical and seismic properties of partially saturated sands

Vanshan Wright[1,2*] and Matthew Hornbach[1]

[1]Southern Methodist University, Roy Huffington Department of Earth Sciences, Dallas, Texas, 75275-0395.

[2]Woods Hole Oceanographic Institution, Department of Geology and Geophysics, Woods Hole, Massachusetts, 02543

*now at

Contents of this file

Text S1
Figures S1 to S5
Tables S1

Introduction

This supplement contains text explaining how we calculated the sedimentation and coastline progradation rates at Port Royal Beach. The supplement also contains figures and tables that present additional results for shoreline progradation rates, mineral fractions, and shear wave velocities in the form of surface wave dispersion curves. The supplement tables the results from using Welch's t-test to assess whether the measured physical properties at Port Royal Beach change with space and time.

Text S1

Constraining Sedimentation and Coastline Progradation Rates

We constrain sedimentation and coastline progradation rates using three-dimensional time contours derived from the beach's paleo shoreline, submarine and subaerial slopes, and sea level. We calculate sedimentation rate as the vertical thickness of the sediments divided by the sediment age, whereas coastline progradation rates are the distances between successively georeferenced shorelines divided by the time taken for the shoreline to prograde to the new distance (Figure 2). These calculations assume a constant depositional rate between mapped contours. This is a simplistic assumption because sedimentation rates tend to be highest while beach sites are at or near sea level, experiencing the full force of both wind and wave-driven sediment transport and deposition. Beach sedimentation rates can also rapidly increase or be eroded during heavy rainfall events. Our sedimentation rates calculations are, therefore, a first-order linear approach, subjected to uncertainties related to our assumption that deposition and progradation rates are constant between mapped contours.

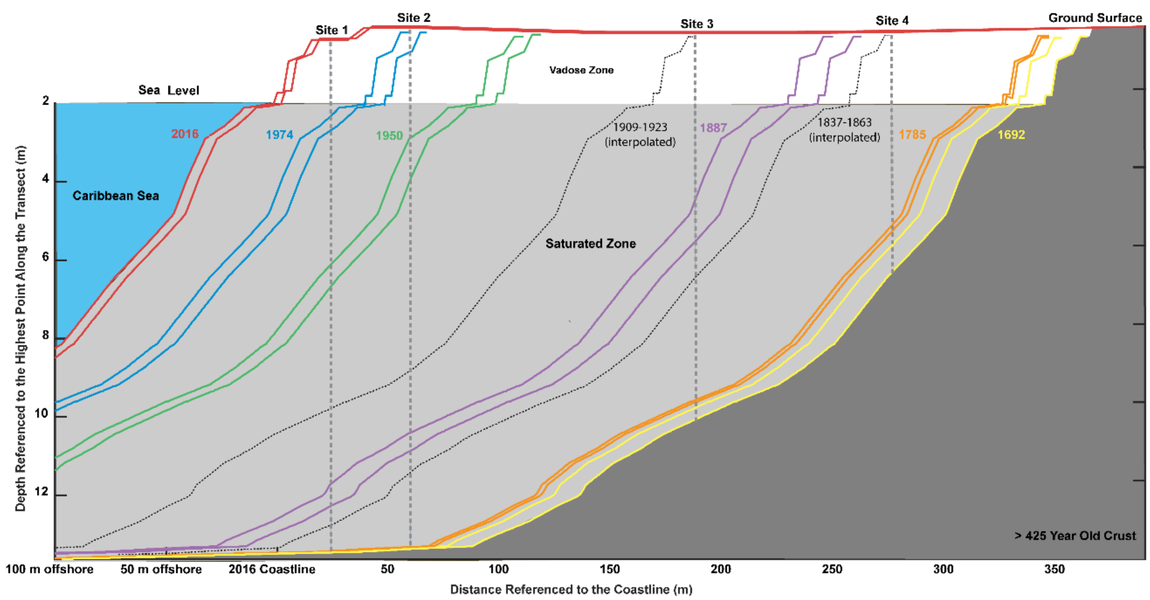

Figure S1. The illustration shows time contours for sediments as a function of depth. Sites 1-4 are highlighted. Sediment ages and sedimentation rates are based on this contoured model. The average calculated sedimentation at site 1-4 was 6-7 cm/year, 9-11 cm/yr, 14-25 cm/year, and 5-11 cm/year, indicating that sedimentation rates were fastest during the deposition of lines 2 and 3.

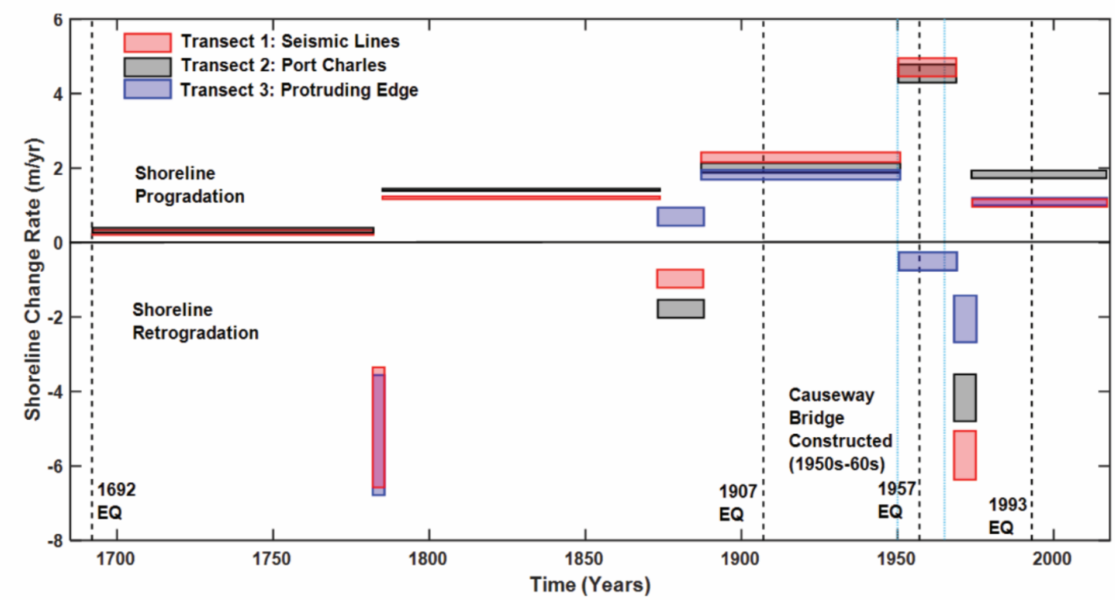

Figure S2. Progradation/retrogradation rate estimates for transect 1-3 delineated in Figure 1 in the main text. The figure includes the timing of significant earthquakes (EQ) in the region. Results show that the shoreline prograding at an average rate of 0.3-0.48 m/year except between the years 1782-1786, 1873-1888, and 1968-1975 which experienced shoreline erosion (Figures 2 and 3).

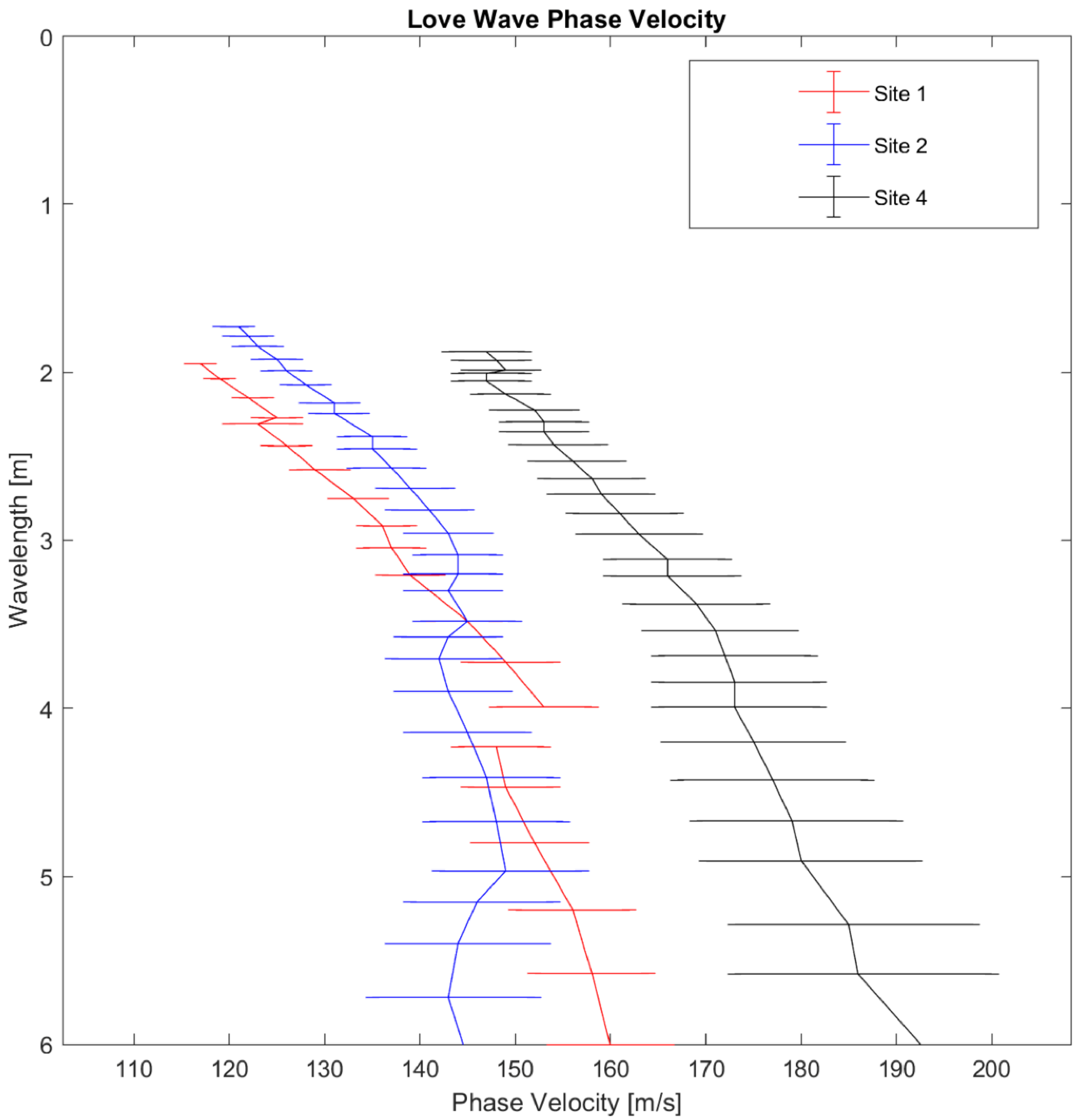

Figure S3. Love wave phase velocities for sites 2-4 at Port Royal Beach Jamaica performed with the phase-shift method. Error bars represent the top 5% of the peak values on the dispersion image.

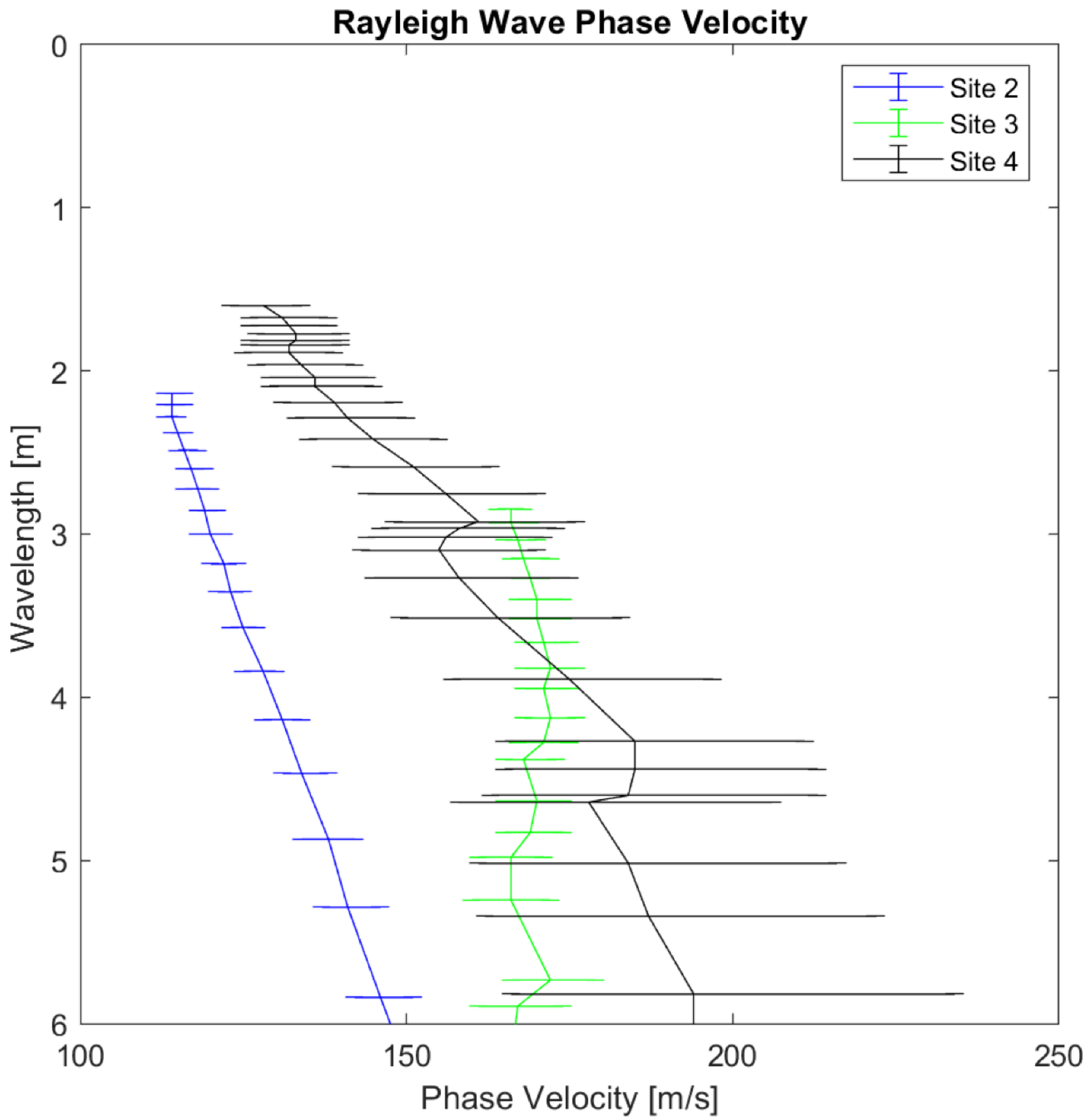

Figure S4. Rayleigh wave phase velocities for sites 2-4 performed with the phase shift method where errors bar represent the top 5% of all values.

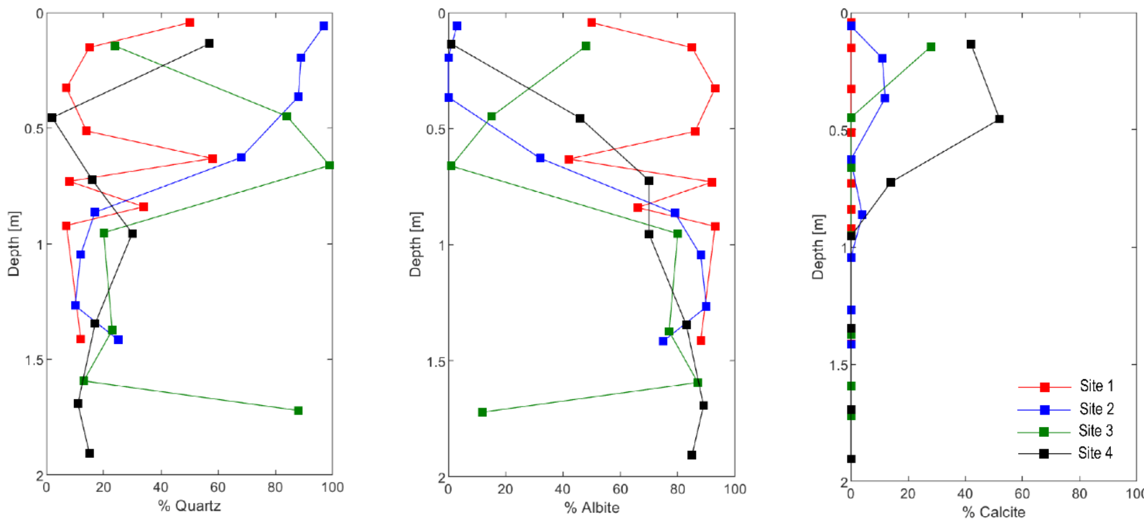

Figure S5. The mineral percentage at sites 1-4 at Port Royal Beach based on X-ray diffraction analyses.

	Welch T-Test Results					Probability that Site 1 is Greater		
Physical Properties	**Highest p**	**Min T**	**Max T**	**Min DF**	**Max DF**	**Site 2**	**Site 3**	**Site 4**
Mineral Bulk Moduli	<< 0.05	-58	36	1.0E+04	1.4E+04	0.82	0.81	0.31
Mineral Shear Moduli	<<0.05	-17	53	9.4E+03	1.6E+04	0.14	0.14	0.57
Cementation	<< 0.05	-43	22	9.4E+03	1.7E+04	0.48	0.66	0.33
Grain size	<<0.05	-54	24	1.4E+04	1.4E+04	0.66	0.39	0.67
Sorting	<<0.05	-31	5	1.3E+04	1.6E+04	0.59	0.59	0.66
Bulk Density	<<0.05	-46	12	1.4E+04	1.7E+04	0.67	0.46	0.65
Porosity	<<0.05	-46	12	1.4E+04	1.7E+04	0.67	0.46	0.65
Pore Fluid	0.9	-2	-2	1.6E+04	1.6E+04	0.50	0.50	0.35
Sphericity	0.08	2	9	1.4E+04	1.6E+04	0.49	0.48	0.46
Roundness	0.0035	3	7	1.4E+04	1.6E+04	0.47	0.49	0.47

Table S1. Results of Welch's T-Test statistics and assessment of the probability that site 1's values are larger than sites 2-4. A probability of 0.5 indicates that the distributions are indistinguishable from each other, within the uncertainties. The labels 'Highest p', 'Min T,' 'Max T,' 'Min DF,' and 'Max DF' refer to the highest p-score, minimum t-score, maximum t-score, minimum degrees of freedom and maximum degrees of freedom related to the Welch's T-Test. The other two (not listed in the table) p-scores for pore fluid, sphericity, and roundness are <<0.05.